Received: 13 February 2019 | Revised: 21 August 2019 | Accepted: 28 August 2019
DOI: 10.1002/eqe.3223

RESEARCH ARTICLE

WILEY

Effects of the improper modeling of viscous damping on the first-mode and higher-mode dominated responses of base-isolated buildings

Hamidreza Anajafi[1] | **Ricardo A. Medina**[2] | **Erin Santini-Bell**[1]

[1] Department of Civil and Environmental Engineering, University of New Hampshire, Durham, NH, USA
[2] Simpson Gumpertz & Heger, Waltham, MA, USA

Correspondence
Hamidreza Anajafi, Department of Civil and Environmental Engineering, University of New Hampshire, Durham, NH, USA.
Email: hamid.anajafi@unh.edu

Funding information
University of New Hampshire

Summary
In many finite element platforms, a classical global damping matrix based on the elastic stiffness of the system (including isolators) is usually developed as part of the solution to the equations of motion of base-isolated buildings. The conducted analytical and numerical investigations illustrate that this approach can lead to the introduction of unintended damping to the first and higher vibration modes and the spurious suppression of the respective structural responses. A similar shortcoming might be observed even when a nonclassical damping model (ie, an assembly of the superstructure and isolation system damping sub-matrices) is used. For example, the use of Rayleigh damping approach to develop the superstructure damping sub-matrix can lead to the undesired addition of damping to the isolated mode arising from the mass-proportional component of the superstructure damping. On the other hand, the improper use of nonclassical stiffness-proportional damping (eg, determining the proportional damping coefficient, β_k, based on the first mode) can result in assigning significant damping to the higher-modes and the unintended mitigation of the higher-mode responses. Results show that a nonclassical stiffness-proportional model in which β_k is determined based on the second modal period of a base-isolated building can reasonably specify the intended damping to the higher modes without imparting undesirable damping to the first mode. The nonclassical stiffness-proportional damping can be introduced to the numerical model through explicit viscous damper elements attached between adjacent floors. In structural analysis software such as SAP2000®, the desired nonclassical damping can be also modeled through specifying damping solely to the superstructure material.

KEYWORDS
base isolation, Rayleigh damping, higher-mode effects, damping leakage, nonlinear modal history analysis, nonlinear direct integration

1 | INTRODUCTION

In a base isolated (BI) building, the superstructure (ie, the section of the structure above the isolation interface) is typically designed to remain in the elastic or near-elastic range during a design earthquake, and the isolation system provides the major source of seismic energy dissipation. As in many other types of structures, in BI buildings, secondary sources of seismic energy dissipation also exist including (i) foundation damping due to soil nonlinearity and radiation of seismic waves; (ii) friction and slippage in steel connections; (iii) opening and closing of micro-cracks in concrete members; (iv) stressing of nonstructural components (eg, partition walls, mechanical equipment, fireproofing, etc.); and (v) friction between structural and nonstructural components, among others. These secondary energy dissipation mechanisms are usually represented by means of an equivalent viscous damping. This type of damping, also known as inherent damping, is typically assumed to be between 1% and 5% of critical damping for different structures. This assumption is mainly based on expert opinion, engineering judgment, and limited system identification studies of buildings that have experienced primarily small-amplitude vibrations (eg, ambient vibration). A few previous studies have illustrated that the traditional use of the inherent damping (eg, the Rayleigh approach) in BI buildings can lead to the introduction of an artificial viscous damping to the isolated (first) mode underestimating the first-mode structural responses, such as isolators displacement demands. This phenomenon is termed as 'damping leakage' in the literature.[1] The present study addresses the effects of the damping leakage phenomenon on the seismic responses of BI buildings with linear and nonlinear isolation systems. In addition to the first-mode dominated responses, which have been the focus of a few previous studies, herein higher-mode dominated responses are also evaluated.

For the response history analysis of BI buildings, modal history and direct integration (DI) analysis methods are usually used. In a modal history analysis, a system of uncoupled equations of motion, which are developed for different structural modes of vibration, is solved. The method of mode superposition is then used to combine the responses of individual modes. On the other hand, the DI method solves the equations of motion in the coupled format using a step-by-step integration. This approach is assumed to provide rather accurate response histories and is widely used in many advanced finite element (FE) packages such as SAP2000®,[2] ETABS®,[3] ABAQUS®,[4] ANSYS®,[5] and OpenSees.[6] However, as shown in this paper and identified in a few previous studies, this premise is not always true. In the modal history analysis approach, the desired inherent damping ratio can be directly specified to the vibration modes of interest (this option is readily available in engineering software platforms such as SAP2000® and ETABS®). Therefore, damping leakage can be prevented by assigning zero damping to the isolated mode,[1] whereas non-zero damping values are specified to other modes to represent the energy dissipation in the superstructure modes. When the DI method is used, a global viscous damping matrix is formed as part of the solution to the equations of motion, which makes it difficult to prevent and control damping leakage. The focus of this paper is mainly on cases for which the equations of motion are solved using the DI method. The rest of this section will address the details of modeling the global damping matrix in the DI approach and the influence of such modeling decisions on the damping leakage phenomenon.

The matrix equation of motion for an n-story BI shear building is given by Equation (1).

$$\mathbf{M}\ddot{\mathbf{x}}(t)+\mathbf{C}\dot{\mathbf{x}}(t)+\mathbf{K}\mathbf{x}(t)+\mathbf{B}F_{\mathrm{b}}(t)=-\mathbf{M}\mathbf{r}\ddot{x}_{\mathrm{g}}(t), \tag{1}$$

$$\mathbf{M}=\begin{bmatrix} m^{\mathrm{b}} & \mathbf{0} \\ \mathbf{0} & \mathbf{M}^{\mathrm{s}} \end{bmatrix}_{(n+1)(n+1)}, \quad \mathbf{C}=\begin{bmatrix} c^{\mathrm{b}}+c_1^{\mathrm{s}} & -c_1^{\mathrm{s}} \\ -c_1^{\mathrm{s}} & \mathbf{C}^{\mathrm{s}} \end{bmatrix}_{(n+1)(n+1)}, \quad \mathbf{K}=\begin{bmatrix} k_1^{\mathrm{s}} & -k_1^{\mathrm{s}} \\ -k_1^{\mathrm{s}} & \mathbf{K}^{\mathrm{s}} \end{bmatrix}_{(n+1)(n+1)}$$

where $\mathbf{x}=\left[x^{\mathrm{b}}x_1^{\mathrm{s}}x_2^{\mathrm{s}}\cdots x_n^{\mathrm{s}}\right]^{\mathrm{T}}$ is the displacement vector of the system relative to the ground. Superscripts 's' and 'b' refer to the superstructure and base-isolators, respectively. $\mathbf{r}$ is a column vector of ones. $\ddot{x}_{\mathrm{g}}$ is the ground acceleration. m^{b} and c^{b} are, respectively, the isolated raft mass and the viscous (inherent) damping coefficient of the isolation systems (eg, the damping coefficient of the rubber compound in elastomeric isolators). $\mathbf{M}^{\mathrm{s}}$, $\mathbf{C}^{\mathrm{s}}$, and $\mathbf{K}^{\mathrm{s}}$ are the mass, viscous damping, and stiffness coefficient matrices of the superstructure, respectively. The constants c_1^{s} and k_1^{s} are the viscous damping and lateral-stiffness coefficients of the superstructure at the first story, respectively. F_{b} is the restoring force provided by the isolators, which in this study is represented by either a bilinear or a linear element. The vector $\mathbf{B}$ = [1, 0, ..., 0]$^{\mathrm{T}}$ gives the position of the isolation system. From Equation (1), it can be seen that the global damping matrix of the system, $\mathbf{C}$, is not a direct superposition of the global stiffness, $\mathbf{K}$, and mass, $\mathbf{M}$, matrices. In other words, the global viscous damping matrix in a BI building is non-proportional (or nonclassical).

For the superstructure of a BI building, assuming a similar viscous damping mechanism throughout the height, classical (proportional) damping applies, and $\mathbf{C}^s$ can be constructed based on the superposition of $\mathbf{M}^s$ and $\mathbf{K}^s$. The $\mathbf{C}^s$ matrix can be also constructed based on modal damping ratios. This study uses the proportional damping approach. Mass-proportional damping (MD), stiffness-proportional damping (KD), and Rayleigh damping (RD) are well-known formulations for this approach; the latter is widely utilized in modeling multi-degrees-of-freedom buildings. The implementation of both the MD and KD models requires assigning a specific superstructure damping ratio, ξ^s, to a single mode (generally the first mode), whereas, in the RD model, specific damping ratios should be assigned to two selected structural modes of vibration. These modes are traditionally the first mode and the mode at which the cumulative modal mass ratio exceeds a relatively large value such as 95% (eg, this mode is the second mode for all isolated and non-isolated buildings used in this study). In a general form of the RD model, damping ratios specified to the two selected modes could be different. However, in this paper, a constant damping ratio is assigned to these two modes. Equations (2a) to (2c) express $\mathbf{C}^s$ for the MD, KD, and RD approaches, respectively:

$$\mathbf{C}^s_{\mathrm{MD}} = \alpha_{\mathrm{m}}\mathbf{M}^s \quad \text{where} \quad \alpha_{\mathrm{m}} = 2\xi^s\omega^*, \tag{2a}$$

$$\mathbf{C}^s_{\mathrm{KD}} = \beta_{\mathrm{k}}\mathbf{K}^s \quad \text{where} \quad \beta_{\mathrm{k}} = 2\xi^s/\omega^*, \tag{2b}$$

$$\mathbf{C}^s_{\mathrm{RD}} = \alpha_{\mathrm{m}}\mathbf{M}^s + \beta_{\mathrm{k}}\mathbf{K}^s \ \text{ where } \ \alpha_{\mathrm{m}} = 2\xi^s\omega_1^*\omega_2^*/\left(\omega_1^* + \omega_2^*\right) \ \text{ and } \ \beta_{\mathrm{k}} = 2\xi^s/\left(\omega_1^* + \omega_2^*\right). \tag{2c}$$

where α_{m} and β_{k} are the constant coefficients of unit s^{-1} and s, respectively. ω^* is the angular frequency corresponding to the mode(s) selected for assigning the intended damping. The physical representations of the KD and MD are shown in Figure 1. The KD component can be interpreted as inter-story dashpots that intend to model the energy dissipation arising from story relative deformations. The MD can be visualized as dashpots attached between the fixed base and each story mass. This latter type of damping, however, is difficult to justify physically.[7] .

Results of the present study show that the assigned (actual) values of damping to the isolated and/or superstructure modes are highly dependent on the approach implemented to model $\mathbf{C}^s$ and, in many cases, deviate from the intended values. As a result, the seismic responses of BI buildings are highly sensitive to the details adopted for modeling the viscous damping. Despite the importance of damping on dynamic responses, a consistent approach is not utilized in the literature for modeling the viscous damping in BI buildings. Many research works dealing with BI buildings (eg, [8-14]) used the RD approach in which the multipliers of mass and stiffness matrices were computed based on the BI modes. Some other works adopted variants of the KD approach (eg, see [15-17]).

The effect of the method of modeling the viscous damping on the seismic responses of BI buildings has not been studied to the level of detail in which this issue has been addressed for non-isolated (NI) structures (for information on modeling the viscous damping in NI structures, the reader is referred to example studies in[18-26]). This discrepancy most likely originates from the notion that energy dissipation provided by the inherent damping mechanisms in BI structures is negligible as compared with the significantly higher energy dissipation of the damping compound of the isolation system. However, it has been shown through a number of studies that the improper modeling of viscous damping can lead to a significant underestimation of BI buildings seismic demands such as base displacement and floor acceleration responses (see [1,23,27-30]). Results of these studies illustrate that the traditional application of RD (ie, Equation (2c) with the elastic stiffness of isolators) could specify an unrealistically high damping to the first-mode of BI structures.

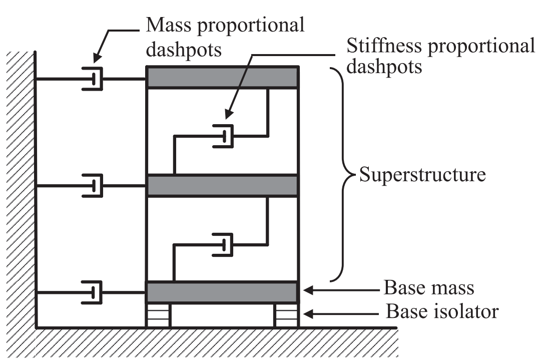

FIGURE 1 Physical representation of the proportional damping models in a base-isolated shear building

A few previous studies have proposed solutions to mitigate the problems associated with modeling viscous damping in BI buildings. For example, for BI buildings with a linear isolation system, Ryan and Polanco[27] showed that using the KD approach and computing β_{k} based on the fundamental mode of the fixed-base superstructure would result in a reasonable specification of damping to the isolated mode. For nonlinear isolation systems, Hall[23] and Pant et al[30] proposed using variants of the KD approach in which the damping matrix was developed based on the post-elastic stiffness of isolators. Kitayama and Constantinou[31] suggested a solution for cases in which the global damping matrix was constructed based on modal damping ratios. In this method, zero damping was specified to the first mode, a constant non-zero damping to the other modes, and the global stiffness of the system was modified to implement the desired stiffness of the isolators for computing the global damping matrix. The aforementioned works were mostly focused on first-mode dominated responses such as isolator displacement. Only the studies conducted by Pant et al[30] and Dao and Ryan,[28] in addition to first-mode responses, considered higher-mode responses such as short-period floor spectral acceleration responses. These two studies were based on comparisons between experimental data and responses from numerical models. For example, Dao and Ryan[28] developed numerical models for a full-scale five-story steel moment frame building that was isolated by triple pendulum bearings. They conducted response history analyses under two ground motion records and concluded that using RD approach along with supplemental damping in the first structural mode could reasonably capture the experimental data. The additional lack of studies addressing the effect of modeling the viscous damping on the higher-mode responses of BI buildings might be due to the notion that in BI buildings the contribution of higher modes is not significant as their mass participation is relatively low. For example, Chopra[7] stated that 'the higher modes [of BI buildings] are essentially not excited by the ground motion—although their [ground] pseudo-accelerations are large—because their modal static responses are very small'. However, as discussed in the early works of Kelly and Tsai[32] and Tsai and Kelly,[33] the coupling between the equations of motion in BI buildings can lead to the presence of significant higher-mode dominated responses. Similarly, the present study also shows that modal mass participation is not a reliable indicator of the relative importance of higher-mode responses in BI buildings. An evaluation of the results of several others studies on BI buildings, available in the literature, can readily reveal the significance of the high-frequency content of floor acceleration responses (eg, see the floor spectra illustrated for tested BI buildings in[28,30] and for numerical BI models in[34-36]).

This study addresses challenges encountered in modeling the viscous (inherent) damping in BI buildings. More specifically, the effect of the phenomenon known as damping leakage on the first- and higher-mode responses of BI buildings is investigated. It is worthwhile noting that in the context of this study, a higher-mode response relates *exclusively* to the short-period floor spectral accelerations. The study includes two main parts. The first part investigates the damping leakage phenomenon in BI buildings with linear isolation systems. In this section, the mathematical models are developed using MATLAB®.[37] The second part deals with BI buildings with bilinear isolation systems. In this second part, the important challenges of modeling a nonclassical viscous damping matrix for BI buildings in FE programs are addressed. The results of the analytical and numerical investigations are used to provide recommendations for the proper modeling of viscous damping in BI buildings.

2 | LINEAR ISOLATION SYSTEMS

The hysteretic energy dissipation of the isolation system is usually incorporated into the numerical model of a BI building through an explicit nonlinear element. However, in particular applications and research studies, a linear spring-dashpot element, with an equivalent damping c^{b} and lateral-stiffness k^{b}, is used to represent the isolation system behavior. The simplicity of linear isolation systems and their fast computation time allow for conducting a large number of numerical simulations to identify behavioral trends. For linear BI buildings, the isolation system restoring force in Equation (1) is given by the equation $F_{\mathrm{b}} = k^{\mathrm{b}}x^{\mathrm{b}}$, and the entire energy dissipation of the isolation system is represented by $c^{\mathrm{b}} = 2\xi^{\mathrm{b}}\omega_1\left(m^{\mathrm{b}} + \sum_1^n m_i^{\mathrm{s}}\right)$, where ξ^{b} is the isolation system (equivalent) damping ratio, and ω_1 is the angular frequency of the first mode of the BI building.

This section primarily evaluates the sensitivity of the structural responses of BI buildings with a linear isolation system (denoted as linear BI buildings hereinafter) to the adopted approach for constructing the superstructure's viscous damping matrix, $\mathbf{C}^{\mathrm{s}}$. Six different scenarios are examined for modeling the $\mathbf{C}^{\mathrm{s}}$ matrix. These scenarios are based on combinations that pair one of the three predefined proportional damping formulations (ie, MD, KD, or RD) with one of the two methods of selecting modal periods (ie, the NI or BI periods) for computing α_{m} and/or β_{k}. Table 1 summarizes the details of the six superstructure various damping models. Modal analyses are performed to evaluate the damping specified by different superstructure viscous damping models to the modal responses of linear BI buildings. Response history analyses are conducted to further verify the results of the modal analyses and propose a damping model that can properly assign the intended damping to the isolated and superstructure modes and, therefore, satisfactorily capture the seismic responses of BI buildings.

2.1 | Predictions of modal analysis for linear base-isolated buildings

2.1.1 | Classical modal analysis

In the first vibration mode (ie, the isolated mode) of a well-designed BI building, the superstructure moves essentially as a rigid body without large inter-story drift motions. Hence, the superstructure viscous damping has a relatively small effect on the damping of a BI building in the first mode. One of the basic premises in this section is that *the damping specified to the first mode of a BI building should be close to the isolation system damping, denoted as the target (intended) first-mode damping herein*. This section estimates the error introduced by different damping models presented in Table 1 to the damping of the first mode of linear BI buildings.

In a BI building, the presence of a nonclassical global damping matrix implies that modal periods, damping ratios, and modal vectors depend not only on the mass and stiffness matrices but also on the damping matrix. As a result, the modal equations are coupled, and classical modal analysis, which neglects the off-diagonal terms of the generalized damping matrix, is not applicable.[7] However, in many studies (eg, [7,27]), the results of classical modal analysis are used to roughly predict the overall behavior of BI systems. This practice is adopted in this section to approximately estimate the viscous damping specified to the vibration modes of linear BI buildings. Ignoring the off-diagonal terms of the transformed matrix, $\mathbf{\Phi}_i^{\mathrm{T}}\mathbf{C}\mathbf{\Phi}_i$, the modal damping ratio at the i-th mode of vibration of a linear BI building is

$$\xi_i = \frac{\mathbf{\Phi}_i^{\mathrm{T}}\mathbf{C}\mathbf{\Phi}_i}{2\omega_i\left(\mathbf{\Phi}_i^{\mathrm{T}}\mathbf{M}\mathbf{\Phi}_i\right)} \quad . \tag{3}$$

where ω_i and the vector $\mathbf{\Phi}_i$ are the i-th circular frequency and i-th mode shape of the BI building, respectively. Assuming that the superstructure behaves as rigid in the isolated mode, $\mathbf{\Phi}_\mathbf{1} = \text{ones}(1, n+1)$. For a general formulation of viscous damping (ie, the RD approach), the superstructure damping matrix is given by the equation $\mathbf{C}^{\mathrm{s}} = \alpha_{\mathrm{m}}\mathbf{M}^{\mathrm{s}} + \beta_{\mathrm{k}}\mathbf{K}^{\mathrm{s}}$. If identical characteristics (ie, story mass, lateral-story stiffness and distribution of viscous damping) are assumed throughout the height of the superstructure, the global damping matrix of the BI building is

$$\mathbf{C} = \begin{bmatrix} c^{\mathrm{b}} + \alpha_{\mathrm{m}} m^{\mathrm{b}} + \beta_{\mathrm{k}} k^{\mathrm{s}} & -\beta_{\mathrm{k}} k^{\mathrm{s}} \\ -\beta_{\mathrm{k}} k^{\mathrm{s}} & \alpha_{\mathrm{m}}\mathbf{M}^{\mathrm{s}} + \beta_{\mathrm{k}}\mathbf{K}^{\mathrm{s}} \end{bmatrix}_{(n+1)(n+1)} . \tag{4}$$

TABLE 1 Superstructure viscous damping models used in this study

Nomenclature	Damping formulation; modes for computing α_{m} and/or β_{k}	Nomenclature	Damping formulation; modes for computing α_{m} and/or β_{k}
MD-NI	Mass-proportional; first NI mode	MD-BI	Mass-proportional; first BI mode
KD-NI	Stiffness-proportional; first NI mode	KD-BI	Stiffness-proportional; first BI mode
RD-NI	Rayleigh; first two NI modes	RD-BI	Rayleigh; first two BI modes

Substituting the respective parameters into Equation (3), the assigned viscous damping to the first mode is

$$\xi_1 = \frac{\mathbf{\Phi}_1^{\mathrm{T}}\mathbf{C}\mathbf{\Phi}_1}{2\omega_1\left(\mathbf{\Phi}_1^{\mathrm{T}}\mathbf{M}\mathbf{\Phi}_1\right)} = \frac{c^{\mathrm{b}} + \alpha_{\mathrm{m}}\left(nm^{\mathrm{s}} + m^{\mathrm{b}}\right)}{2\omega_1\left(nm^{\mathrm{s}} + m^{\mathrm{b}}\right)} = \frac{c^{\mathrm{b}}}{2\omega_1\left(nm^{\mathrm{s}} + m^{\mathrm{b}}\right)} + \frac{\alpha_{\mathrm{m}}}{2\omega_1}. \tag{5}$$

The first term in Equation (5) is basically the target (intended) damping at the isolated mode, ξ^{b}, and therefore the second term is the additional (unintended) damping denoted as ξ_1^{error} herein. This error term is produced by the mathematical procedure adopted for modeling the global damping matrix. As seen, the value of ξ_1^{error} is independent of the coefficient β_{k}, meaning that the KD component does not impart an extra damping to the first mode of a linear BI building (ie, the KD-NI and KD-BI models introduce no damping error to the first mode). In other words, the incorporated error is the exclusive result of the MD component. This conclusion can be also intuitively drawn from an evaluation of Figure 1. The MD dashpots shown in this figure are activated when the building vibrates in the isolated mode. Therefore, the MD component introduces damping to the isolated mode that is beyond the damping provided by the isolation system (these observations corroborate the results of Ryan and Polanco[27]).

Table 2 illustrates the value of the ξ_1^{error} parameter for the six different superstructure viscous damping models evaluated in this section. The value of the ξ_1^{error} associated with the MD-NI and RD-NI models is a function of the fraction $\omega_1^{\mathrm{s}}/\omega_1$ (ie, the ratio of the frequency of the first mode of the NI superstructure to that of the BI building). This latter observation implies that the greater the separation between the fundamental frequency of the NI superstructure and of the isolation system, the larger the difference between the first-mode damping ratio and the target value. This conclusion was also reported by Ryan and Polanco[27] through the modal damping analysis of example BI buildings. The fraction $\omega_1^{\mathrm{s}}/\omega_1$ for the practical range of BI buildings is usually greater than 3.0. Therefore, the lower bound value of ξ_1^{error} produced by the MD-NI model is $3.0\xi^{\mathrm{s}}$. Assuming $\omega_2^{\mathrm{s}} = 3\omega_1^{\mathrm{s}}$, which is the case for regular moment resisting frame systems and also for the linear shear building studied next, the minimum value of ξ_1^{error} for the RD-NI model is $2.3\xi^{\mathrm{s}}$. The MD-BI and RD-BI models lead to a ξ_1^{error} whose value is limited to ξ^{s} (note that for the practical range of BI buildings, the fraction $\omega_2/(\omega_2+\omega_1)$ tends to unity). The above mentioned results suggest that among the considered methods, the KD approach, regardless of whether β_{k} is determined based on the NI or BI fundamental frequency, can reliably specify the intended damping to the isolated mode of a linear BI building.

2.1.2 | Generalized modal analysis

In this section, generalized modal analysis[7] is conducted for representative linear BI buildings with isolated periods, T^{b}, of 1.8, 3.0, and 4.2 s and different superstructure-isolator damping ratios. For all BI configurations, the superstructure is a six-story shear frame with identical characteristics in all stories and a fixed-base fundamental period, T^{s}, of 0.6 s. The mass of the isolation system is assumed to be the same as the typical story mass. Isolator-superstructure damping combinations that pair two different ξ^{s} values of 5% and 10% and three different ξ^{b} values of 5%, 15%, and 30% are examined. Characteristics such as the 5% damping for the isolation system and the 10% inherent damping for the superstructure, although unrealistic, are used as extreme cases for comparison purposes.

The analysis results show that, for the studied BI configurations, the modal mass participation ratios of the higher modes are relatively small (ie, less than 1%). However, as illustrated in this section and identified by a few previous studies (eg, [38]), modal mass participation ratio may not be a reliable predictor of the importance of higher-mode responses in a BI building because of the coupling of the modal equations. Table 3 illustrates the estimated modal damping ratios of the first three modes for the BI buildings assuming different damping models. As seen, the estimated modal damping ratio for the isolated mode (first mode) by the KD-NI and KD-BI models in all configurations is close to the first-mode target damping ratio, whereas the other four damping models result in greater first-mode damping ratios than those

TABLE 2 The value of the ξ_1^{error} parameter for the six superstructure viscous damping models

Damping model	ξ_1^{error}	Damping model	ξ_1^{error}
MD-NI	$\xi^{\mathrm{s}}\omega_1^{\mathrm{s}}/\omega_1$	MD-BI	ξ^{s}
KD-NI	0	KD-BI	0
RD-NI	$\xi^{\mathrm{s}}\omega_1^{\mathrm{s}}\omega_2^{\mathrm{s}}/\left[\omega_1\left(\omega_1^{\mathrm{s}}+\omega_2^{\mathrm{s}}\right)\right]$	RD-BI	$\xi^{\mathrm{s}}\omega_2/(\omega_2+\omega_1)$

TABLE 3 Estimated modal damping ratios for different superstructure viscous damping models

Damping	T^b = 1.8 (s)				T^b = 3.0 (s)				T^b = 4.2 (s)			
		Modal damping %				Modal damping %				Modal damping %		
model	Config.	ξ_1	ξ_2	ξ_3	Config.	ξ_1	ξ_2	ξ_3	Config.	ξ_1	ξ_2	ξ_3
MD-NI	ξ^s = 5%	19.2	4.3	2.2	ξ^s = 5%	29.7	3.7	1.8	ξ^s = 5%	39.8	3.4	1.7
KD-NI	ξ^b = 5%	4.3	10.6	18.6	ξ^b = 5%	4.7	10.1	18.4	ξ^b = 5%	4.9	9.9	18.3
RD-NI		15.4	5.9	6.3		23.4	5.3	6.0		31.0	5.1	5.9
MD-BI		9.2	2.5	1.2		9.7	1.6	0.7		9.8	1.1	0.5
KD-BI		4.6	28.5	54.3		4.9	46.6	90.2		4.9	65.0	126.1
RD-BI		8.5	6.4	9.1		9.2	5.9	9.4		9.5	5.7	9.5
MD-NI	ξ^s = 5%	27.5	7.6	3.7	ξ^s = 5%	39.1	5.7	2.8	ξ^s = 5%	49.5	4.9	2.4
KD-NI	ξ^b = 15%	12.6	13.9	20.2	ξ^b = 15%	14.1	12.2	19.3	ξ^b = 15%	14.5	11.4	18.9
RD-NI		23.7	9.2	7.9		32.8	7.4	7.0		40.7	6.5	6.6
MD-BI		17.5	5.9	2.8		19.1	3.6	1.6		19.5	2.6	1.2
KD-BI		12.9	31.8	55.9		14.2	48.7	91.1		14.6	66.4	126.8
RD-BI		16.8	9.7	10.7		18.6	8.0	10.3		19.2	7.1	10.1
MD-NI	ξ^s = 5%	40.0	12.6	6.0	ξ^s = 5%	53.2	8.8	4.1	ξ^s = 5%	64.1	7.1	3.3
KD-NI	ξ^b = 30%	25.1	18.9	22.5	ξ^b = 30%	28.2	15.2	20.7	ξ^b = 30%	29.1	13.6	19.9
RD-NI		36.2	14.2	10.2		46.9	10.4	8.3		55.2	8.7	7.5
MD-BI		30.0	10.9	5.1		33.2	6.7	3.0		34.1	4.8	2.1
KD-BI		25.4	36.8	58.2		28.3	51.7	92.5		29.2	68.6	127.8
RD-BI		29.3	14.7	13.0		32.7	11.0	11.7		33.7	9.3	11.1
MD-NI	ξ^s = 10%	34.2	6.9	3.5	ξ^s = 10%	54.7	6.4	3.2	ξ^s = 10%	74.8	6.1	3.1
KD-NI	ξ^b = 5%	4.5	19.5	36.5	ξ^b = 5%	4.8	19.3	36.4	ξ^b = 5%	4.9	19.1	36.3
RD-NI		26.6	10.1	11.9		42.0	9.6	11.6		57.1	9.4	11.5
MD-BI		14.2	3.4	1.7		14.7	2.1	1.0		14.8	1.5	0.7
KD-BI		5.0	55.3	107.9		5.0	92.3	180.0		5.0	129.2	252.0
RD-BI		12.8	11.1	17.5		13.8	10.8	18.3		14.1	10.6	18.7

intended implying the leakage of the superstructure damping to the isolated mode. These results are consistent with those of Section 2.1.1.

The second premise used in this study is that *the second mode of a BI building is controlled by the superstructure mass and stiffness, and, as a result, the damping ratio of this mode should be comparable with the superstructure viscous damping ratio at its first few modes*. As consistently seen in Table 3, the resulting higher-mode damping ratios are highly sensitive to the adopted approach for constructing $\mathbf{C}^s$. For example, for the BI building with $T^b = 3.0$ s, $\xi^s = 5\%$, and $\xi^b = 15\%$, the estimated second-mode damping by different approaches varies from 3.6% to 48.7% implying a significant sensitivity. It is also apparent that, for all BI configurations, the MD models provide the lower-bound estimates of the higher-mode damping, which in many cases are smaller than the target values. An evaluation of the results reveals the presence of an apparent leakage of the isolation system damping to the damping of the higher modes. For all damping models, as the isolation system damping increases while other parameters are unchanged, the specified damping to the higher modes significantly increases. For example, consider the modal damping ratios of the MD-BI model for the configurations with $T^b = 3.0$ s and $\xi^s = 5\%$. In this case, increasing the isolation system damping from 5% to 30% results in an increase in the second-mode damping ratio from 1.6% to 6.7%. The results of response history analyses of Section 2.2 illustrate that only when the isolation system damping is low (ie, the leakage of the isolation system damping to the superstructure modes is insignificant), the estimated higher-mode damping ratios shown in Table 3 are meaningful (ie, correlated with the amplitude of the higher-mode seismic responses). An evaluation of the damping ratios for such cases illustrates that only the RD-NI and RD-BI models can specify reasonable damping values to the higher-modes. One can interpret that the KD-NI and KD-BI models (ie, the models that provide reliable first-mode damping ratios) fail to assign the intended damping to the higher modes. As seen in Table 3, even when the value of the isolation system damping is not significant, the apparent higher-mode damping ratios estimated by these models are significantly greater than the intended values.

The results of this section illustrate that using the proportional damping approaches to model the superstructure viscous damping can lead to the introduction of an artificial damping to the vibration modes of BI buildings. It is evident that, in this case, if a modal history analysis method is used to solve the equations of motion, the structural responses can be significantly underestimated. The next section investigates whether these superstructure damping models lead to similar drawbacks when a DI response history analysis method is conducted. The correlations of the estimated damping ratios with the structural responses are also investigated (eg, if an apparent large value of damping of the higher-mode predicted by a damping model is associated with a significant mitigation of the higher-mode responses). The results are used to introduce a damping model that can reliably capture the first- and higher-mode responses of BI buildings.

2.2 | Sensitivity of the responses of linear base-isolated buildings to the superstructure viscous damping model

This section investigates the effect of the choice of the superstructure viscous damping model on the seismic responses of linear BI buildings when the DI method is used to solve the equations of motion. Preliminary analyses illustrate that the extent of this effect depends on the characteristics of input ground motion records.[39] Therefore, in this section, response history analyses are conducted using a set of 20 far-field ground motions, and mean responses are evaluated to address this record-to-record variability. A total of 30 six-story BI building models are developed based on different combinations of the following structural parameters: T^b/T^s = (3.0:1.0:7.0), ξ^s = (2%, 5%), and ξ^b = (5%, 15%, 30%). For all configurations, T^s = 0.60 s is assumed. For a given BI configuration, six different variants are evaluated, which correspond to the six different superstructure viscous damping models introduced in Table 1. Hence, for a structural response of interest, six different mean values are obtained from the response history analyses. The extent of the variation in these mean values can illustrate the sensitivity of a structural response to the choice of the superstructure viscous damping model.

Floor acceleration spectra can illustrate the significance of different structural modes simultaneously and, therefore, are used for the initial evaluations conducted in this section. Subsequently, additional engineering demand parameters (EDPs) are evaluated to further verify the results. Floor spectra are generally used for the estimation of seismic demands on nonstructural components. In the section, for developing floor spectra, the component period, T_c, is varied from 0 to $1.5T^b$. The assumed component damping ratio is 2% that is a reasonable value for most typical nonstructural components.[40] Figures 2A–C illustrate the mean 2%-damped roof pseudo-spectral acceleration (FSa) responses for three representative BI structures with the same isolated period of 1.8 s but different ξ^s and/or ξ^b values, exposed to the 20 far-field ground motion records. The configuration shown in Figure 2C with unrealistic values of damping is presented for comparison purposes.

An evaluation of Figure 2 illustrates that for a given roof-spectrum period, especially for periods in the vicinity of the modal periods of the BI buildings, the variation between the estimated values of FSa obtained from different viscous damping models is significant. The MD and RD models (especially the MD-BI) do not lead to a significant suppression

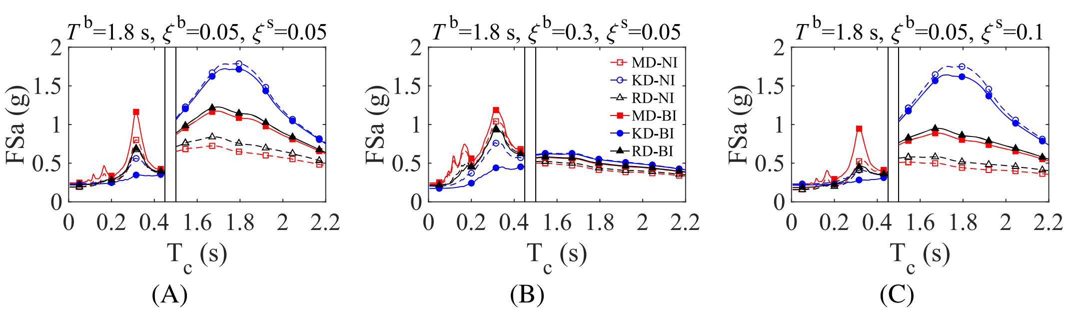

FIGURE 2 Mean 2%-damped roof pseudo-acceleration spectra of the BI configurations with an isolated period of 1.8 s for different superstructure damping models [Colour figure can be viewed at wileyonlinelibrary.com]

of the floor spectral ordinates in the vicinity of the higher modes but significantly mitigate the floor spectral values in the vicinity of the fundamental mode. An opposite trend is observed for the KD models. These observations are consistent with the results of Section 2.1.2 where it was shown that, for example, the KD methods assign a reasonable first-mode damping but a fictitiously large second-mode damping to the vibration modes of a linear BI building. An evaluation of the floor spectral values in the vicinity of the second mode suggests that the RD models provide a more reasonable estimate of higher-mode responses, as discussed next. It is well-understood that when the isolation system damping is relatively low (eg, 5%), the superstructure and isolated raft are essentially decoupled. In this condition, given the relatively high stiffness of the superstructure with respect to the isolation system, the superstructure's behavior is consistent with that of a semi-rigid body (ie, close to a single-degree-of-freedom system). Therefore, for such a BI configuration, the higher-mode dominated responses (ie, spikes in the short-period range of the roof spectra) should be relatively small. When, in addition to the low damping of the isolation system, the superstructure is highly damped (eg, 10% as considered in Figure 2C), the superstructure relative deformations decrease even more, and the superstructure tends to experience rigid-body translation. In this case, higher-mode effects are significantly mitigated. On the other hand, when the isolation system damping is relatively large (eg, Figure 2C), due to the coupling of the vibration modes, the higher mode effects are expected to be considerable. An evaluation of Figures 2A–C illustrates that the RD models more reasonably meet these expectations.

A comparison of the floor spectra presented in Figures 2A and B reveals that the coupling effect, which is amplified by the isolation system damping, can impart seismic energy to the higher modes. This is consistent with the findings of Kelly and Tsai[32] and Hall[41] for far-field ground motions. As seen, with increasing the isolation system damping from 5% (Figure 2A) to 30% (Figure 2B), for a given damping model (except for the MD-BI), the floor spectral ordinates in the vicinity of the second mode increase. For example, this increase for the RD-BI model is from 0.69 g to 0.93 g. From the results of modal analysis (Table 1), it is observed that increasing the isolation system damping increases the higher-mode damping values. The results of the present section illustrate that correlations do not exist between the estimated higher-mode damping values and the magnitudes of the higher-mode responses as the greater higher-mode damping ratios are associated with greater responses rather than smaller responses. In other words, the increased damping ratios due to the high value of the isolation system damping are fictitious (or apparent). This important conclusion illustrates that the results of modal analysis for the higher-mode damping are meaningful (ie, correlated with higher-mode responses) only when the isolation system damping is low.

The sensitivity of three different EDPs to the choice of the superstructure viscous damping model is evaluated next for many BI configurations with different characteristics. For a given EDP and structural model, six different mean values are obtained from analysis subject to a single ground motion record. These six values are normalized to the value of the EDP for the KD-NI model. This normalization facilitates the understanding of the variation in the values of the EDP due to the superstructure viscous damping model. The three considered EDPs are peak base drift (PBD), peak roof acceleration (PRA), and peak component acceleration (PCA) responses. Most typical nonstructural components are situated in the period range [0-0.5] s.[39] On the other hand, the higher modal periods of the BI configurations studied herein are smaller than 0.5 s. In the present section, the maximum value of the roof spectral acceleration ordinates across the period range [0-0.5] s is referred to as the PCA and is a representative of the higher-mode responses.

Figure 3A illustrates the mean normalized PBD responses of different BI buildings for the considered damping models, assuming a fixed ξ^s value of 2%. In this figure, the R parameter is the period ratio, T^b/T^s. Figure 3B presents similar results for the BI buildings with $\xi^s = 5\%$. As consistently seen, the mean PBD estimates of the KD-NI and KD-BI methods are very close to one another and govern those of the other damping models. The mean PBD responses for the RD-BI and MD-BI methods are fairly close to one another and are up to 20% below those estimated when

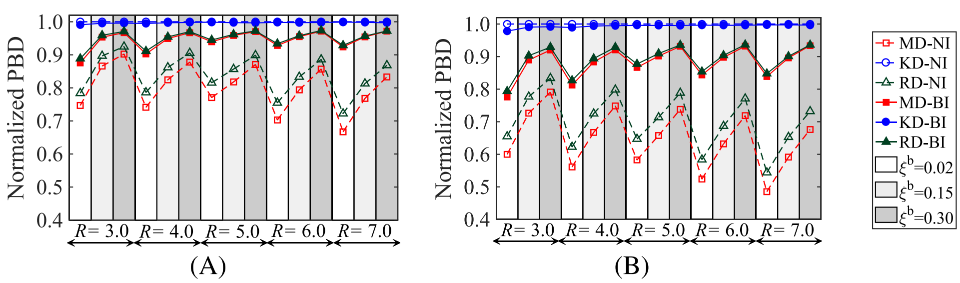

FIGURE 3 Mean normalized peak base drift responses for different superstructure damping models: (A) $\xi^s = 2\%$; (B) $\xi^s = 5\%$ [Colour figure can be viewed at wileyonlinelibrary.com]

applying the KD-NI approach (see Figure 3B). The mean PBD estimates of the MD-NI and RD-NI methods are up to 60% smaller than those of the KD-NI. These observations are consistent with the trend identified in the first-mode damping ratio in Section 2.1. An evaluation of Figures 3A and 3B illustrates that with increasing the value of ξ^s, the sensitivity of the PBD responses to the damping model increases.

Figures 4A and B demonstrate, respectively, the variation of the mean normalized PRA and PCA responses for the BI configurations with $\xi^s = 5\%$. Figure 4A reveals that for the configurations with ξ^b within the practical range (ie, $\xi^s = 15\%$ and 30%), the KD-BI, which provides the near upper-bound estimates of the PDB, results in the lower-bound PRA responses. Figure 4B shows that the KD-BI and MD-BI provide the lower- and upper-bound estimates of the PCA responses, respectively. For configurations with characteristics within the practical range (ie, $R \geq 3.0$ and $\xi^b \geq 15\%$), the mean normalized PCA responses obtained from analysis with different damping models could vary from 0.35 to 2.5, which illustrates that higher-mode responses are highly sensitive to the choice of the superstructure damping model. In general, with increasing ξ^b while keeping the other structural parameters constant, the sensitivity of the mean estimates of the considered EPDs to the damping model tends to decrease (ie, less variation is observed). On the contrary, for most cases, an increase in the value of T^b while keeping the other parameters constant, causes an amplification in the variation of the mean EDPs.

2.3 | Recommendations for modeling the superstructure viscous damping in linear base-isolated buildings

In the previous section, it was shown that the traditional use of the RD models (ie, specifying the intended damping either to the first two modes of the fixed-base superstructure or BI building) can provide reasonable estimates of higher-mode responses but this approach underestimates the first-mode responses arising from the MD component. The KD component of the superstructure inherent damping does not impart undesirable damping to the isolated mode of the BI buildings, regardless of the mode used for determining the proportional damping coefficient, β_k. However, it was shown that the traditional use of the KD as recommended in previous studies (ie, determining β_k based on the first modal period of the fixed-base superstructure or the BI building) would introduce significant additional (and unintended) damping to the higher-modes, and, as a result, in many cases, higher-modes responses are virtually damped out. In this section, it is shown that the KD approach, when used properly, could provide a reasonable estimate of the higher-mode responses of linear BI buildings. In essence, the higher mode effects in a BI building are due to the superstructure inter-story deformations. To mitigate the higher-mode responses of a BI building without significantly altering the first-mode responses, proper inter-story dampers are needed. By definition, the KD component of the superstructure inherent damping is meant to simulate this suppression. The second mode of the BI building is essentially the first superstructure mode. This mode controls the inter-story drift motions for the studied buildings. Therefore, a reasonable approach for the suppression of higher modes is to implement the KD and assign the intended superstructure damping to the second mode of the BI building. Results illustrate that this approach, for the low-damping isolation systems (where the results of modal analysis are meaningful), results in a second mode damping close to the intended one. For example, modal analysis illustrates that for the configuration with $T^b = 1.8$ s, $\xi^s = 10\%$, and $\xi^b = 5\%$, the estimated second mode damping by this approach is 11% (ie, very close to the intended ξ^s), and for the configuration with $\xi^s = 5\%$ and $\xi^b = 5\%$, this value is 6.3%. Further analyses show that if ξ^b is close to zero (ie, the case without the leakage of the

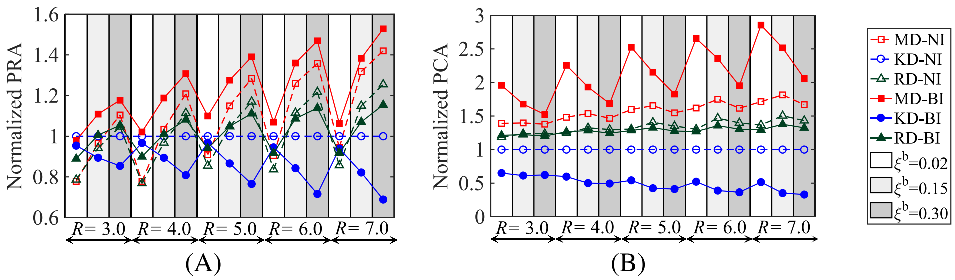

FIGURE 4 (A) Mean normalized peak roof acceleration responses; (B) Mean normalized peak component acceleration responses; for different superstructure damping models ($\xi^s = 5\%$) [Colour figure can be viewed at wileyonlinelibrary.com]

isolation system damping to the superstructure modes), the estimated second-mode damping by this approach tends to ξ^s.

Figure 5 presents an evaluation of the proposed KD-BI approach using the mean roof acceleration spectra of three representative BI buildings. As seen, the response estimate of the proposed approach in the vicinity of the first mode is fairly close to that of the traditional KD (ie, the intended response). In the vicinity of the higher modes, the floor spectral acceleration responses captured by the proposed KD-BI are in between the upper-bound (ie, the estimation of the MD-BI) and the lower-bound responses.

The short-period floor spectral acceleration responses are used to estimate seismic demands on nonstructural components whose integrity and operability are of paramount importance. Therefore, it might be reasonable (and conservative) to consider the upper-bound estimates as the intended responses. An evaluation of the simulation results illustrates that with simple modifications with respect to the traditional application, the RD-BI model can approximately capture the upper-bound estimates of both higher-mode and first-mode responses. In this approach, for a linear shear-type BI building with a total of n horizontal degrees of freedom, the two selected modal frequencies for assigning ξ^s are $\omega_1/2$ and ω_n rather than the widely used ω_1 and ω_2 (ie, the first two angular frequencies of the BI building). With respect to the traditional RD, this approach reduces the damping specified to the BI modes, and, as a result, the response estimates tend to the upper bound values. The results of this method are also shown in Figure 5.

3 | BILINEAR ISOLATION SYSTEMS

This section investigates the effects of the improper modeling of viscous damping on the seismic responses of BI buildings with bilinear isolation systems. For the analyses conducted in this section, the FE models are developed in the SAP2000® interface. Although the modeling procedure in SAP2000® is highlighted, most of the presented methodologies and discussions are also applicable to other FE software packages. Results of nonlinear response history analyses are used to propose practical approaches for the proper modeling of viscous damping in BI buildings with bilinear isolators.

3.1 | Nonlinear direct integration versus fast nonlinear analysis

Nonlinear DI (NLDI) and nonlinear modal time-history analysis, also known as fast nonlinear analysis (FNA),[42] are widely used for the response history analysis of BI buildings (eg, SAP2000® offers both methods). The NLDI approach solves the complete set of equilibrium equations (ie, the coupled equations of motion) at every time step. In this approach, if a system becomes nonlinear, it may be necessary to reassemble the stiffness matrix for the complete structural system at each time step. Also, iterations may be required within each time increment to achieve convergence and satisfy equilibrium. Therefore, this method is computationally intensive.[42] In the FNA approach, element nonlinear responses are treated as unbalanced forces that are grouped with external loads.[43] This method reduces the large set of global equilibrium equations to a relatively small number of uncoupled second order differential equations. As a result, the FNA has the advantage of much faster computational time as compared with the NLDI. Furthermore, as first identified by Sarlis and Constantinou[1] and corroborated in this section, another advantage of the FNA over the NLDI method is the inherent ability of this approach to control the phenomenon of damping leakage in BI buildings. In the FNA approach, contrary to the NLDI, a matrix equation of motion including a global damping matrix is not solved, and, instead, modal damping ratios are directly applied to the uncoupled modal equations. For example, the FNA

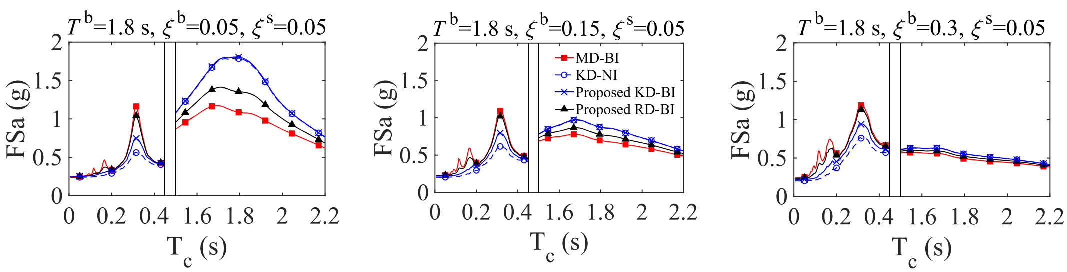

FIGURE 5 Evaluation of the proposed viscous damping models based on the mean 2%-damped roof pseudo-acceleration spectra of three representative linear BI building configurations [Colour figure can be viewed at wileyonlinelibrary.com]

method in SAP2000® gives the user the ability to assign the global values of viscous damping for all modes, and, at the same time, damping ratios can be manually overridden for a number of modes. Therefore, the damping leakage phenomenon can be readily prevented by specifying a 0% damping to the isolated mode, whereas non-zero damping values are assigned to the other modes.[1] In the NLDI approach, as discussed in Section 2, due to the existence of a global damping matrix, the mitigation of damping leakage is more challenging. It is worth noting that in the FNA approach, special considerations should be given for selecting a sufficient number of Ritz vector modes and also incorporating global P-Δ effects (see Sarlis and Constantinou[1] for details). In SAP2000®, this method is mostly applicable when the number of nonlinear elements is limited, and they are modeled using a nonlinear link element.

3.2 | Damping leakage for an example bilinear base-isolation system studied in this paper

A five-span four-story isolated frame is used herein to evaluate damping leakage due to different viscous damping models in BI buildings with bilinear isolation systems. The superstructure, which is adopted from a BI building presented in Sarlis and Constantinou,[1] is a two-dimensional slice of an actual steel moment resisting frame with rigid beam-column connections. The seismic weight of each story is 4804 kN, which is equally distributed across a floor level as lumped masses at beam-column joints. The periods of the first three modes of the fixed-base superstructure are 0.78, 0.25, and 0.14 s. It is assumed that the superstructure is supported on six lead rubber bearings (LRBs). A floor with the same weight as the typical floors' weight is added right above the isolation interface. Two types of LRBs with different characteristics are examined. In the first type of the LRB, the ratio of the yield strength of the total of the six LRBs to the superstructure's seismic weight, F_y/W, is 0.05, and the yield displacement of the LRBs, x_y, is 10 mm. For the second type, these values are 0.10 and 20 mm, respectively (as seen, the two LRB types have the same initial stiffness). The post-elastic stiffness of the LRBs, k_{pe}^{b}, is 10% of their elastic (initial) stiffness, k_{el}^{b}. These characteristics are within typical ranges used in practice. The periods of the first three modes of the isolated frame computed based on k_{pe}^{b} are 2.91, 0.45, and 0.22 s. The isolated building configurations are excited by three ground motions recorded at distances more than 10 km from the rupture fault: *ABBAR-T*: the east-west component of the 1990 Manjil earthquake (magnitude 7.4) recorded at Abbar station; *GO3090*: the east-west component of the 1999 Loma Prieta earthquake (magnitude 6.9) recorded at Gilroy Array #3 station; and *YER360*: the north-south component of the 1992 Landers earthquake (magnitude 7.3) recorded at Yermo Fire station. The PGA of the individual records is scaled to 0.60 g, which is the design PGA assuming a site of high seismicity in California, USA. Figure 6 illustrates the scaled 5%-damped pseudo-acceleration spectra of the three selected ground motion records.

3.3 | Damping leakage in the fast nonlinear analysis method

The damping leakage to the isolated mode introduced by the FNA method was first identified by Sarlis and Constantinou.[1] They showed that the stiffness of the isolators used for the modal analysis has a significant effect on this phenomenon. In some available FE platforms, this stiffness could be adjusted to be different than the initial stiffness of the isolators. For example, in SAP2000®'s implementation of the FNA, modal damping ratios are specified to the

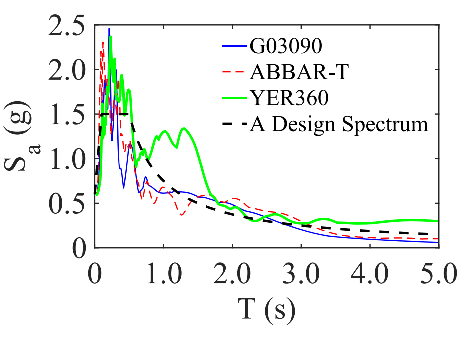

FIGURE 6 Amplitude-scaled 5%-damped pseudo-acceleration response spectra of the selected ground motion records along with a design spectrum for a site of high seismicity [Colour figure can be viewed at wileyonlinelibrary.com]

vibration modes that are computed based on a predefined isolator stiffness, referred to as the 'effective stiffness' in the characteristics of the rubber isolator element. Although the value of this effective stiffness remains constant throughout the response, it can be selected to be significantly smaller than the initial stiffness of isolators. This section, while corroborating the results of Sarlis and Constantinou,[1] extends the discussion to the higher-mode dominated responses. More specifically, the effects of the value of the structural parameters including the stiffness of the isolators used for modal analysis (ie, the introduced effective stiffness in SAP2000®), the yield strength of the isolators, and also the specified viscous damping on the extent of damping leakage to the isolated mode and superstructure modes are investigated. Two different input effective stiffness, $k^{\mathrm{b}}_{\mathrm{eff}}$, values are used: the elastic stiffness and post-elastic stiffness of the isolators (ie, $k^{\mathrm{b}}_{\mathrm{el}}$ and $k^{\mathrm{b}}_{\mathrm{pe}}$). Overall, three different analysis cases are examined: (i) damping for all modes is 0%; (ii) damping for all modes is 5% and $k^{\mathrm{b}}_{\mathrm{eff}} = k^{\mathrm{b}}_{\mathrm{pe}}$; and (iii) damping for all modes is 5% and $k^{\mathrm{b}}_{\mathrm{eff}} = k^{\mathrm{b}}_{\mathrm{el}}$. The analysis case with 0% damping assigned to all modes is considered as the baseline for the evaluation of the first-mode damping leakage. Figure 7A illustrates the normalized base shear versus the base displacement response obtained from different analysis cases for the BI configuration with $F_{\mathrm{y}}/W = 0.10$ subject to the scaled ABBAR-T record. Figure 7B presents similar results for the configuration with $F_{\mathrm{y}}/W = 0.05$.

An evaluation of Figure 7, consistent with the results of Sarlis and Constantinou,[1] illustrates that the damping leakage phenomenon is more pronounced when the elastic stiffness of the LRBs is used for modal analysis. For the considered case study, the elastic stiffness of the LRBs is 10 times their post-elastic stiffness. Therefore, for the analysis case with $k^{\mathrm{b}}_{\mathrm{el}}$, when the LRBs experience inelastic actions, the generated viscous damping force in the isolated mode would be relatively large with respect to the isolators shear force. As a result, the peak base displacement (PBD) and peak normalized base shear ($V_{\max}/W$) demands are significantly underestimated. For example, in Figure 7B, the PBD response for the baseline case with no damping leakage is 0.44 m. For this configuration, the damping leakage phenomenon in the analysis cases with $k^{\mathrm{b}}_{\mathrm{pe}}$ and $k^{\mathrm{b}}_{\mathrm{el}}$ causes the PBD response to reduce to 0.30 m (ie, 32% underestimation) and 0.20 m (ie, 55% underestimation), respectively. For these two analysis cases, the $V_{\max}/W$ demand is underestimated by 25% and 46%, respectively. As seen, the underestimation of the response in the analysis case with $k^{\mathrm{b}}_{\mathrm{el}}$ is more significant. It is also observed that the adverse effect of damping leakage is more highlighted for the configuration with a lower yield strength, F_{y}. For example, for the configuration with $F_{\mathrm{y}}/W = 0.10$, damping leakage in the analysis with $k^{\mathrm{b}}_{\mathrm{el}}$ results in reducing the PBD from 0.22 m to 0.15 m (ie, 32% underestimation), whereas for $F_{\mathrm{y}}/W = 0.05$, as discussed above, this underestimation is as large as 55%. This observation is further elaborated next. Equation (6) can approximate the equivalent damping ratio, $\xi^{\mathrm{b}}_{\mathrm{eq}}$, generated by the hysteretic behavior of the LRBs[44]:

$$\xi^{\mathrm{b}}_{\mathrm{eq}} = \frac{2\,(1-\alpha)(\mu-1)}{\pi\mu[1+\alpha(\mu-1)]}. \tag{6}$$

where μ is the shear displacement ductility ratio defined as the ratio of the isolator maximum displacement response to the isolator yield displacement, and α is the isolator post-elastic stiffness ratio, $k^{\mathrm{b}}_{\mathrm{pe}}/k^{\mathrm{b}}_{\mathrm{el}}$. The response for the analysis cases with 0% damping (ie, with no damping leakage) are used to estimate the value of $\xi^{\mathrm{b}}_{\mathrm{eq}}$ for each LRB type. Substituting the respective quantities in Equation (6), for the configurations with $F_{\mathrm{y}}/W = 0.05$ and 0.10, the value of $\xi^{\mathrm{b}}_{\mathrm{eq}}$ is 11%

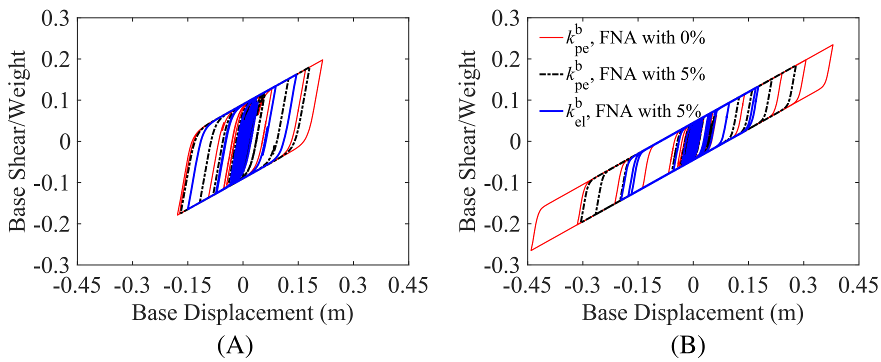

FIGURE 7 Force-displacement loops of the BI building subject to the scaled ABBAR-T record for different analysis cases: (A) $F_{\mathrm{y}}/W = 0.10$; (B) $F_{\mathrm{y}}/W = 0.05$ [Colour figure can be viewed at wileyonlinelibrary.com]

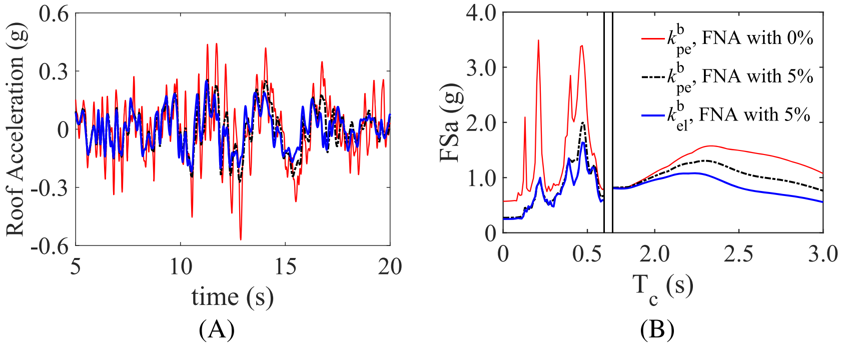

FIGURE 8 (A) Roof acceleration time histories and (B) 2%-damped roof pseudo-acceleration spectra of the BI building with $F_y/W = 0.05$ subject to the scaled ABBAR-T record for different analysis cases [Colour figure can be viewed at wileyonlinelibrary.com]

and 26%, respectively. As seen, ξ^b_{eq} for the configuration with $F_y/W = 0.05$ is much smaller, and, hence, the seismic responses for this configuration are more influenced by the damping leakage. Similar analyses are performed assuming modal damping ratios other than 5%. Results illustrate that the damping leakage phenomenon is much more pronounced when the specified modal damping is higher. For example, for the configuration with $F_y/W = 0.05$ subject to the scaled ABBAR-T record, damping leakage in the analysis case with k^b_{el} and 2% damping would reduce the PBD from 0.44 m to 0.28 m (ie, 36% underestimation), whereas, as discussed previously, this underestimation for the analysis case with k^b_{el} and 5% damping is up to 55%.

Figures 8A and B illustrate, respectively, the roof acceleration time histories and the 2%-damped roof acceleration spectra for the configuration with $F_y/W = 0.05$ subject to the scaled ABBAR-T record, assuming different damping scenarios. As seen in Figure 8A, the roof acceleration responses for the analysis case with 0% damping assigned to all modes are significantly greater than those for the two analysis cases with 5% damping. It is observed that, when a 5% damping is assigned to all modes, the roof acceleration responses are weakly sensitive to the selection of k^b_{el} or k^b_{pe}. Similar conclusions can be drawn from the evaluation of the roof spectra shown in Figure 8B. In addition, Figure 8B reveals that in the analysis case with 0% damping assigned to all modes, the floor spectral acceleration responses in the vicinity of the higher modes are unrealistically large because these modes are virtually undamped.

To further verify the abovementioned observations, similar analyses are performed on the BI configuration with $F_y/W = 0.10$ subject to the scaled GO3090 record, and the results are presented in Table 4 for four different damping scenarios: (i) 0% damping is specified to all modes; (ii) 0% damping is specified to the first mode and 5% to the higher modes; (iii) 5% damping is assigned to the first mode and 0% damping to the higher modes; and (iv) 5% damping is assigned to all modes. For each damping scenario, the analyses are performed when the input k^b_{eff} value is either set equal to k^b_{el} or k^b_{pe}, resulting in a total of eight analysis cases. The results presented in Table 4 mainly corroborate those obtained from the analyses subject to the ABBAR-T record. Additional observations are discussed next. When a nonzero damping is assigned to the isolated mode, the PBD and V_{max}/W responses are strongly dependent on the value of the input k^b_{eff}, whereas with assigning a zero damping to the isolated mode, these EDPs are weakly dependent on the value of k^b_{eff}. For a given damping scenario (rows 1 to 4), the PRA and PCA responses are not very sensitive to the choice of k^b_{eff}. An evaluation of the results also reveals that the PRA response is not significantly influenced by the first structural mode because when the first-mode damping increases from 0% to 5% and other modal damping ratios remain unchanged, the amplitude of the PRA response is not meaningfully altered (compare the PRA responses in the first and third rows of Table 4). On the contrary, this EDP is highly affected by the higher modes because, for example,

TABLE 4 Evaluation of EDPs obtained from the FNA using different modeling approaches for the BI building with $F_y/W = 0.10$ subjected to the scaled GO3090 record

	V_{max}/W		PBD (m)		PRA (g)		PCA (g)	
Specified modal damping	k^b_{el}	k^b_{pe}	k^b_{el}	k^b_{pe}	k^b_{el}	k^b_{pe}	k^b_{el}	k^b_{pe}
0% to all modes	0.26	0.26	0.34	0.34	0.66	0.66	4.80	4.80
0% to 1st mode; 5% to higher modes	0.25	0.26	0.32	0.33	0.46	0.48	2.24	2.65
5% to 1st mode; 0% to higher modes	0.22	0.24	0.26	0.30	0.63	0.65	4.37	4.24
5% to all modes	0.21	0.24	0.25	0.30	0.46	0.47	2.48	2.20

in the analysis case with k_{pe}^{b} when the higher-mode damping is increased from 0% to 5% and the first-mode damping is fixed at 0%, the PRA reduces from 0.66 g to 0.48 g (compare the PRA responses in the first and second rows of Table 4).

Results of this section suggest that applying the FNA method with 0% first-mode damping override and a constant non-zero higher-mode damping can be considered a reasonable solution to prevent damping leakage to the isolated mode and simultaneously provide reliable higher-mode responses. This approach is selected as a baseline to evaluate the response estimates of other approaches presented in the next sections.

3.4 | Damping leakage in the direct integration analysis method

In the NLDI method, the proportional damping is usually used to model the inherent damping of a structure. In this approach, the global inherent damping matrix in many cases is constructed through applying the proportional damping coefficients to the global stiffness and mass matrices of the system. For example, this is the case when the proportional damping is introduced through the Load Case in SAP2000®. Implementing this method implies that the nonclassical aspect of the global damping matrix of a BI building is not maintained. On the other hand, in many FE software packages, by default, the elastic stiffness of the isolator (ie, the stiffness of the element at zero initial conditions regardless of its current nonlinear state), k_{el}^{b}, is used to develop the global damping matrix. The combination of these two issues could potentially amplify damping leakage to the first mode of a BI building. The accuracy of this statement is examined through a simplified formulation presented next. Assume that a nonlinear isolation system at a given time instant can be represented by an effective stiffness, k_{eff}^{b}, and an effective damping, c_{eff}^{b}. Assuming a classical RD based on the elastic stiffness of the system, the global inherent damping matrix is given by $\mathbf{C}' = \alpha_m \mathbf{M} + \beta_k \mathbf{K}_{el}$, where $\mathbf{K}_{el}$ is the elastic global stiffness matrix of the BI building. Incorporating the isolation system effective damping into $\mathbf{C}'$, the global (equivalent) $\mathbf{C}$ matrix is

$$\mathbf{C} = \begin{bmatrix} c_{eff}^{b} + \alpha_m m^{b} + \beta_k k_{el}^{b} + \beta_k k^{s} & -\beta_k k^{s} \\ -\beta_k k^{s} & \alpha_m \mathbf{M}^{s} + \beta_k \mathbf{K}^{s} \end{bmatrix}_{(n+1)(n+1)}. \tag{7}$$

Assuming that the superstructure moves as a rigid body in the isolated mode, Equation (3) is used to compute the assigned damping to the first mode of the BI building:

$$\xi_1 = \frac{c_{eff}^{b} + \left(nm^{s} + m^{b}\right)\alpha_m + \beta_k k_{el}^{b}}{2\omega_1\left(nm^{s} + m^{b}\right)} = \frac{c_{eff}^{b}}{2\omega_1\left(nm^{s} + m^{b}\right)} + \frac{\alpha_m}{2\omega_1} + \frac{\beta_k k_{el}^{b}}{2\omega_1\left(nm^{s} + m^{b}\right)}. \tag{8}$$

The first term in Equation (8) is basically ξ_{eff}^{b} (ie, the intended first-mode damping), and the two other terms are the error introduced to the isolated-mode damping. Letting $N = \omega_2/\omega_1$, the RD coefficients are

$$\alpha_m = 2\xi^{s}\omega_1 \frac{N}{N+1} \quad \text{and} \quad \beta_k = \frac{2\xi^{s}}{\omega_1}\frac{1}{N+1}. \tag{9}$$

Substituting α_m and β_k into Equation (8), the first-mode damping error is

$$\xi_1^{error} = \xi^{s}\frac{N}{N+1} + \frac{\xi^{s} k_{el}^{b}}{(\omega_1)^2\left(nm^{s} + m^{b}\right)}\frac{1}{N+1}. \tag{10}$$

In Equation (10), the term $(\omega_1)^2(nm^{s} + m^{b})$ is the effective stiffness of the isolation system, k_{eff}^{b}, and hence, the error term can be expressed by Equation (11).

$$\xi_1^{error} = \xi^{s}\frac{N}{N+1} + \xi^{s}\frac{k_{el}^{b}}{k_{eff}^{b}}\frac{1}{N+1}. \tag{11}$$

The second term in Equation (11) is proportional to the fraction k_{el}^{b}/k_{eff}^{b}. As seen, because k_{el}^{b} is used for developing the $\mathbf{C}$ matrix, the incorporated damping error is relatively large. For example, for a BI building with effective periods of

$T_1 = 3.0$ and $T_2 = 0.50$ s, and $k_{\text{el}}^{\text{b}}/k_{\text{eff}}^{\text{b}} = 8.0$ (which are selected based on the case study of Section 3.3), the adopted approach results in $\xi_1^{\text{error}} = 2.0\xi^{s}$. For this example, using $k_{\text{eff}}^{\text{b}}$ for developing the **C** matrix in Equation (7), which is not simple in a platform such as SAP2000®, would replace the $k_{\text{el}}^{\text{b}}/k_{\text{eff}}^{\text{b}}$ ratio by unity resulting in $\xi_1^{\text{error}} = \xi^{s}$.

Following a similar methodology, one can show that if the classical KD model with the initial stiffness of the isolators is used for developing the **C** matrix in Equation (7), the value of ξ_1^{error} can be obtained by Equation (12). In this case, for the abovementioned BI building example, the value of ξ_1^{error} is $8.0\xi^{s}$, which implies a significant damping leakage. This observation suggests that the traditional use of the KD in a platform such as SAP2000® can result in a significant underestimation of first-mode responses. However, if the KD model based on $k_{\text{eff}}^{\text{b}}$ is used for computing the **C** matrix, the fraction $k_{\text{el}}^{\text{b}}/k_{\text{eff}}^{\text{b}}$ in Equation (12) is replaced by unity, and the ξ_1^{error} parameter would default to ξ^{s}.

$$\xi_1^{\text{error}} = \xi^{s} k_{\text{el}}^{\text{b}}/k_{\text{eff}}^{\text{b}} \quad . \tag{12}$$

In the rest of this section, the damping leakage in the NLDI approach is investigated using the case study BI building presented in Section 3.3. For the numerical analyses in this section, the intended viscous damping is specified to the effective modes of the BI buildings (ie, the modes with periods computed based on k_{pe}^{b}). Hereinafter, for brevity, the term 'effective' is removed from the expression 'effective mode'. An approach adopted in an analysis example provided in the SAP2000®'s verification manual for bilinear isolators is also examined. In this approach, for the NLDI analysis, a variant of the classical KD is used in which β_{k} is computed based on the second modal period of the BI building. This method intends to limit the viscous damping specified to the first and higher modes. For example, for the case of the BI building studied herein, assuming a viscous damping ratio of 5%, the traditional use of the KD (ie, β_{k} based on the first modal period) results in assigning 5% and 32% damping to the first and second modes, respectively. However, if the KD variant proposed by the SAP2000®'s verification manual is used, these quantities are close to 1% and 5%, respectively. The results of the FNA with 0% first-mode damping override (introduced as the baseline in Section 3.3) are used for the evaluation of the accuracy of the analysis cases investigated herein. For the analyses conducted in this section, unless mentioned otherwise, (i) the value of the specified viscous damping is 5%; (ii) the proportional damping coefficients are applied to the structure as a whole (ie, defined through the Load Case in SAP2000®) implying a classical damping; and (iii) for the RD method, the intended viscous damping is specified to the first two modes of the BI building.

Figure 9A illustrates the normalized base shear versus the base displacement for the configuration with $Q_{\text{y}}/W = 0.05$ exposed to the scaled ABBAR-T record, assuming different analysis cases. The results of the NLDI approach with three damping models including the traditional RD, the traditional KD, and the KD proposed by SAP2000® are presented along with the results of the baseline case. Results presented in Figure 9A, consistent with those of the analytical solution provided earlier in this section, illustrate that using the NLDI method with the traditional KD leads to a significant first-mode damping leakage and consequently the underestimation of the PBD and V_{max}/W responses by 73% and 60%, respectively. These underestimations for the NLDI analysis cases with the traditional RD are 47% and 40%, and with the SAP2000®' modified KD approach are 40% and 33%, respectively. As seen, determining β_{k} based on the second mode instead of the first mode mitigates the adverse effects of damping leakage inherent in the classical KD; however, the remaining damping leakage is still significant. An additional variant of the classical RD in which 0% damping is specified to the first mode and 5% to the second mode is also examined. The results (omitted for brevity) show that for the configuration with $F_{\text{y}}/W = 0.05$ subjected to the scaled ABBAR-T and GO3090 ground motions, applying this variant of the RD method leads to an underestimation of the PBD by 41% and 31%, respectively. Figure 9B illustrates the 2%-

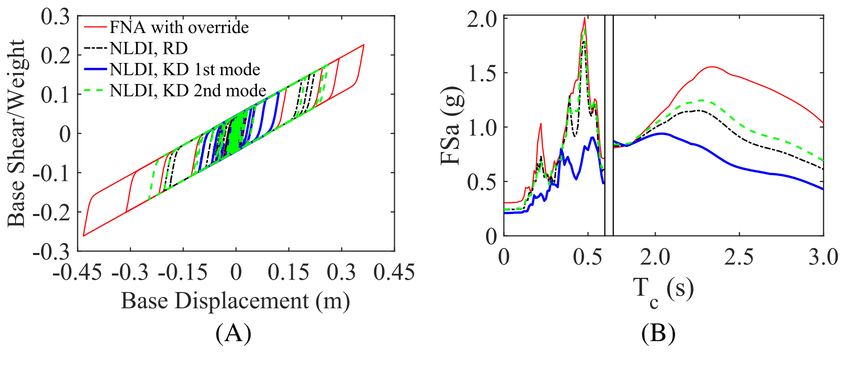

FIGURE 9 (A) Force-displacement loops and (B) 2%-damped roof pseudo-acceleration spectra of the BI building with $F_{\text{y}}/W = 0.05$ subject to the scaled ABBAR-T record for different analysis cases [Colour figure can be viewed at wileyonlinelibrary.com]

damped roof acceleration spectra for the four analysis cases introduced above. It is observed that the response estimates of the NLDI method with the traditional RD and modified KD models for the floor spectral ordinates in the vicinity of the second mode are close to those of the FNA approach with damping override. Nevertheless, the traditional KD model leads to a significant underestimation of these responses. It is also evident that none of the three NLDI variants can provide a reasonable estimation of the floor spectral ordinates in the vicinity of the first mode.

3.5 | Proposed solutions to eliminate the shortcomings associated with modeling viscous damping in the direct integration analysis method

When using the NLDI approach for the response history analysis of a BI building, a nonclassical viscous damping matrix should be developed. The mathematical model used to develop this matrix should be able to (i) prevent the leakage of the superstructure damping to the isolated mode and (ii) accurately specify the intended superstructure damping to the higher modes. To achieve the first objective in FE platforms that by default construct a global classical damping matrix (eg, SAP2000®), the global proportional damping coefficients (eg, those introduced through the Load Case menu in SAP2000®) should be set equal to zero. As illustrated by Sarlis and Constantinou,[1] this approach can satisfactorily capture the first-mode responses (eg, see Figure 10A); however, it cannot provide a reasonable estimate of the floor acceleration responses. As seen in Figure 10B, this approach leads to unrealistically larger short-period floor acceleration responses as it leaves the higher modes (superstructure modes) virtually undamped. This section proposes solutions for this latter shortcoming.

In Section 2.3, it was discussed that the KD component of the superstructure mitigates the higher-mode responses (superstructure responses) in a BI building. For the i-th story, the desired horizontal damping force provided by the KD term of the superstructure damping can be expressed by Equation (13).

$$\left(F_i^{\mathrm{vd}}\right)_x = \beta_{\mathrm{k}} k_i^{\mathrm{s}} \left(\dot{x}_i^{\mathrm{s}} - \dot{x}_{i-1}^{\mathrm{s}}\right). \tag{13}$$

In Equation (13), $\dot{x}_i^{\mathrm{s}}$ is the horizontal velocity of the i-th floor with respect to the ground; k_i^{s} is the lateral stiffness of the i-th story defined herein as the load (story shear-force) required to produce a unit displacement of a subassembly consisting of the i-th story's columns fixed at the bottom end and the beams above; $\beta_{\mathrm{k}} = 2\xi^{\mathrm{target}}/\omega_2$, where ξ^{target} is the intended viscous damping ratio (eg, 0.05), and ω_2 is the second angular frequency of the BI building computed based on the post-elastic stiffness of the isolators. In an FE platform, explicit viscous damping elements attached between the adjacent floors can generate the desired damping force given by Equation (13). The details of modeling these viscous damping elements in an analysis program such as SAP2000® are provided next. In SAP2000®, the Exponential Maxwell Damper element, denoted as the viscous damper (VD) hereinafter, can be adjusted to generate the damping force given by Equation (13). This element includes a dashpot in series with a linear spring. The nonlinear force-velocity relationship of the VD can be expressed as

$$F^{\mathrm{vd}} = k^{\mathrm{vd}} \Delta = C^{\mathrm{vd}}\, \dot{d}^{\lambda}. \tag{14}$$

where k^{vd} is the spring stiffness; C^{vd} is the damping coefficient; Δ is the deformation across the spring; $\dot{d}$ is the deformation rate across the dashpot; and λ is the damping exponent. Theoretically, for a given story, every span of the frame

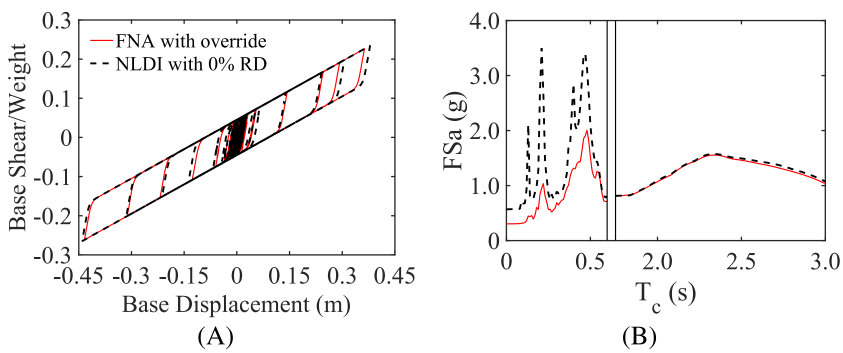

FIGURE 10 Evaluation of the NLDI analysis case with 0% damping using the responses of the BI building with $F_y/W = 0.05$ subject to the scaled ABBAR-T record: (A) force-displacement loops; (B) 2%-damped roof pseudo-acceleration spectra [Colour figure can be viewed at wileyonlinelibrary.com]

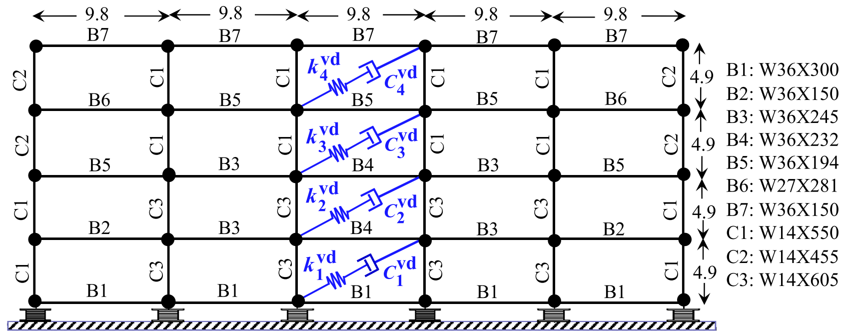

FIGURE 11 Schematic view of the base-isolated four-story frame with the proposed viscous damper elements (dimensions in meters) [Colour figure can be viewed at wileyonlinelibrary.com]

should be equipped with identical VDs to represent a uniform distribution of the inherent damping throughout the story. However, as illustrated later in this section, for the studied BI buildings, the axial force demands on the attached VDs are not significant with respect to the columns' gravity forces (ie, the local effects are insignificant). Furthermore, in the FE model used in this study, the horizontal displacements of all nodes of a given floor are constrained together. Therefore, it is reasonable to assume that a single VD attached at the middle span of a story of the frame can represent the entire inherent damping in the story. Figure 11 illustrates the schematic model of the four-story BI building with the proposed VDs attached diagonally between the adjacent floors. To minimize the axial deformations of the spring component of the VDs and obtain the behavior desired for the purpose of this study (ie, pure damping), a relatively large value is assigned to k^{vd}. Therefore, the total deformation of the VD element would be the deformation of the dashpot, d. For the i-th story, $\dot{d}_i \approx \left(\dot{x}_i^{\mathrm{s}} - \dot{x}_{i-1}^{\mathrm{s}}\right)\mathrm{Cos}(\theta_i)$, where θ_i is the angle the attached VD makes with the horizontal. The horizontal component of the VD force should simulate the KD force given by Equation (13). Therefore, the λ exponent should be equal to unity, and the damping coefficient C_i^{vd} should satisfy Equation (15).

$$C_i^{\mathrm{vd}} = \beta_{\mathrm{k}} k_i^{\mathrm{s}} / \mathrm{Cos}^2(\theta_i). \tag{15}$$

As an illustrative example, for the studied four-story frame, $k_1 = 4.06{\times}10^5$ kN/m; $\theta_1 = 0.46$ rad; and assuming a viscous damping ratio of 5%, $\beta_{\mathrm{k}} = 7.2{\times}10^{-3}$ s. Substituting these parameters into Equation (15), C_1^{vd} is equal to $3.64{\times}10^3$ kN-s/m.

The proposed VDs are incorporated into the FE model, and NLDI analyses are conducted for the three scaled ground motion records. Figure 12A illustrates the axial force-deformation loops of the attached VD at the first story for the BI configuration with $F_{\mathrm{y}}/W = 0.10$ subjected to the scaled ABBAR-T record. Figure 12B presents similar results for the BI configuration with $F_{\mathrm{y}}/W = 0.05$. As seen in Figures 12A and B, for both configurations, the axial force of the VD element is limited to $0.01W$. The horizontal component of this force is $9.0{\times}10^{-3}W$, which is significantly smaller than the building maximum base shear (ie, $0.26W$). The summation of the vertical components of the VDs forces at all stories is limited to $0.04W$, whereas the gravity force of the column adjacent to the VDs is 0.17 W implying that VDs alter the

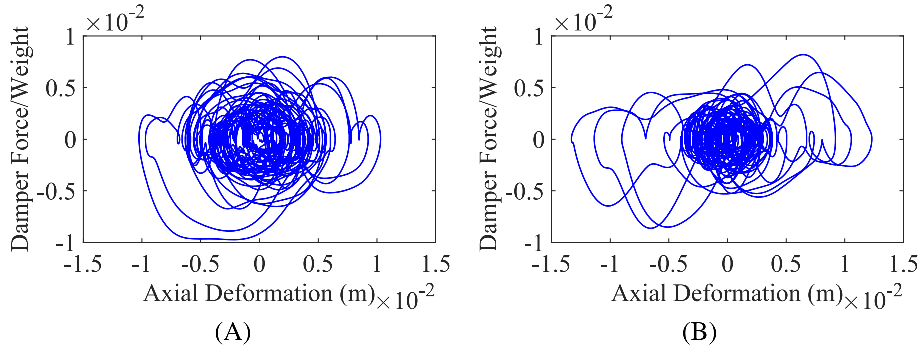

FIGURE 12 Axial force-deformation hysteretic loops for the attached viscous damper at the first story of the BI building subject to the scaled ABBAR-T record: (A) $F_{\mathrm{y}}/W = 0.10$; (B) $F_{\mathrm{y}}/W = 0.05$ [Colour figure can be viewed at wileyonlinelibrary.com]

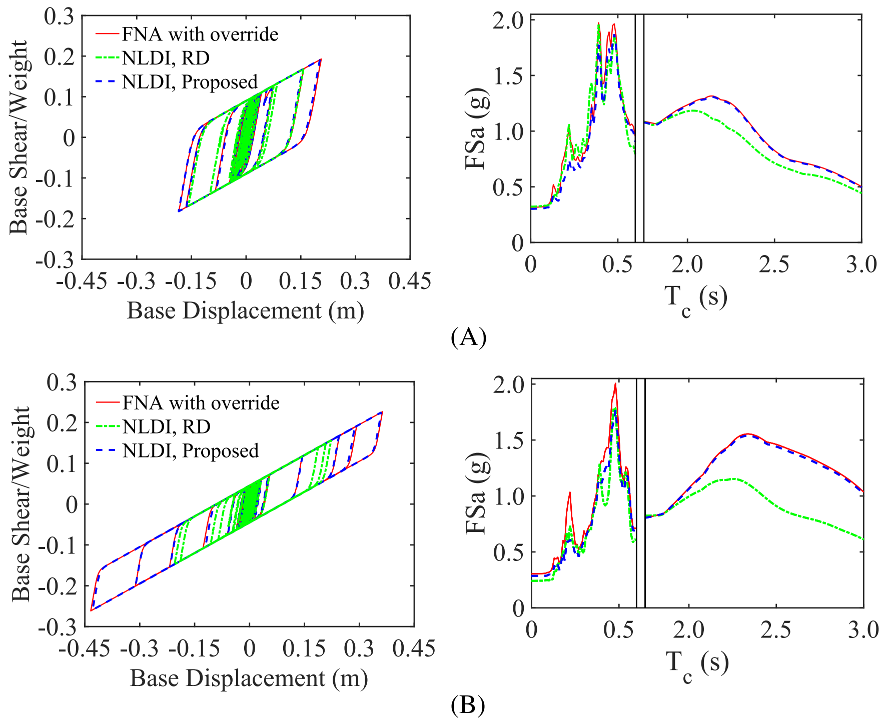

FIGURE 13 Evaluation of different analysis cases using the responses of the two BI building configurations subject to the scaled ABBAR-T record: (A) $F_y/W = 0.10$; (B) $F_y/W = 0.05$ [Colour figure can be viewed at wileyonlinelibrary.com]

column maximum axial force by only 10%. Therefore, the local effect of the VDs is not significant. Furthermore, given the load combinations used for designing structural elements (eg, those used in ASCE/SEI 7-16[45]) and the relatively small seismic forces generated by these supplementary VDs, gravity loads are to govern the design of the considered columns. If for a given BI building, the axial force of the VD elements is significant, the VDs should be distributed at every span of the frame to minimize their local and global effects.

Figure 13 presents an evaluation of the proposed approach using the responses of the two BI configurations to the scaled ABBAR-T record. In this figure, in addition to the results of the proposed approach and the baseline case (the FNA with damping override), the results for the NLDI approach with 5% traditional RD (5% global damping to the first two modes of the BI building) are also presented for comparison purposes. As seen, the NLDI with 5% RD underestimates structural responses, especially first-mode responses, with respect to the baseline case (eg, see isolator displacement and shear force responses in Figure 13B). The results consistently illustrate that the response estimates of the proposed approach, especially the peak responses that are usually used for design proposes, are fairly close to those of the baseline case. The estimates of the proposed methods for the floor spectral accelerations in the vicinity of the second mode, which dominate the floor spectrum, and also in the vicinity of the first mode closely match those of the baseline case. The baseline case specifies a constant 5% viscous damping to the second and higher modes. However, in the proposed approach, the KD coefficient was computed based on specifying 5% damping to the second mode, and therefore, a higher damping value is automatically specified to the third and higher modes. As a result, the estimates of the spectral acceleration responses in the vicinity of the third and higher modes based on the proposed approach are lower than those of the baseline case.

An alternative solution is also proposed that might be software-specific and not available in some FE platforms. In SAP2000®, a nonclassical damping matrix that does not alter the first-mode damping can be developed using 'material damping'. In this software, the intended viscous damping can be specified to the materials of interest (instead of the Load Case). This allows for the specification of the viscous damping only to the superstructure material in a BI building. Adopting this approach, the proportional damping coefficients are not applied to the global stiffness and mass matrices of the BI building but instead are applied to the superstructure elements, and as a result, a nonclassical damping matrix is developed. The accuracy of this method is examined in Figures 14A and 14B. As seen, this approach results in base-shear hysteresis loops and roof spectral acceleration ordinates that are analogous to those of the FNA approach with damping override.

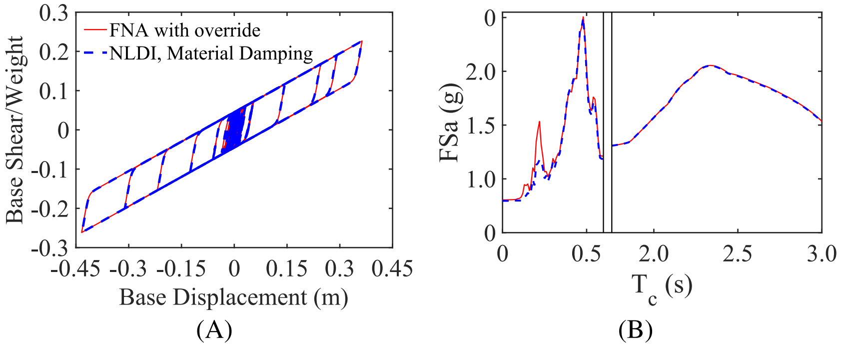

FIGURE 14 Evaluation of the NLDI analysis case with material damping using the responses of the BI building with $F_y/W = 0.05$ subject to the scaled ABBAR-T record: (A) force-displacement loops; (B) 2%-damped roof pseudo-acceleration spectra [Colour figure can be viewed at wileyonlinelibrary.com]

TABLE 5 The values of the selected seismic responses of the BI configuration with $F_y/W = 0.05$ subject to the three ground motions records for different analysis cases

Event	The scaled ABBAR-T					The scaled GO3090					The scaled YER360				
		NLDI [b]					NLDI					NLDI			
	FNA [a]	RD5	RD0	Mat.	VD	FNA	RD5	RD0	Mat.	VD	FNA	RD5	RD0	Mat.	VD
V_{max}/W	0.26	0.16	0.27	0.26	0.26	0.26	0.20	0.26	0.25	0.26	0.27	0.23	0.27	0.27	0.27
PBD (m)	0.43	0.22	0.44	0.43	0.43	0.42	0.30	0.42	0.42	0.42	0.44	0.37	0.45	0.44	0.44
PRD (m)	0.48	0.26	0.50	0.48	0.48	0.48	0.33	0.49	0.48	0.48	0.50	0.42	0.51	0.50	0.50
PRA (g)	0.31	0.24	0.58	0.30	0.29	0.37	0.31	0.56	0.36	0.34	0.39	0.31	0.53	0.37	0.35
PCA (g)	2.0	1.8	3.4	2.0	1.8	2.0	1.6	4.4	1.9	1.8	2.1	2.1	4.6	2.1	1.9

Note: (a) FNA with 0% first-mode damping override and 5% higher-mode damping (the baseline case). (b) NLDI approach with four different damping models: RD5 and RD0 imply, respectively, RD with 5% and 0% damping for the first two modes of the BI building; the term 'VD' refers to the proposed approach with 0% damping together with the additional VDs; the acronym 'Mat.' implies 5% KD assigned to the superstructure material.

Table 5 presents the values of various seismic responses of the configuration with $F_y/W = 0.05$ subject to the three scaled ground motion records for different analysis cases including the NLDI approach with the proposed damping models (ie, the supplemental VDs and material damping). Results presented in this table consistently illustrate that both proposed approaches can provide responses fairly close to those of the baseline analysis case, whereas, the NLDI method with the widely used 5% RD can significantly underestimate both first- and higher-mode dominated responses.

4 | CONCLUSIONS

This study addresses challenges encountered in modeling the viscous (inherent) damping in base-isolated (BI) buildings with linear and bilinear isolation systems. The conducted numerical and analytical investigations illustrate that the mathematical method adopted for the Finite Element (FE) modeling and analysis of a BI building can lead to the unintended addition of damping to the vibration modes of the building. It is shown that this phenomenon, referred to as 'damping leakage', can result in a significant underestimation of the first- and/or higher-mode responses. Direct Integration (DI) and modal history analysis are widely used for the response history analysis of BI buildings. When a modal history analysis is used, the global inherent damping could be directly specified to the vibration modes of interest. Therefore, as identified in a previous study[1] and corroborated in this research, damping leakage can be readily prevented by assigning a zero damping to the isolated mode, whereas the desired non-zero damping values can be assigned to the higher modes. For example, this feature is available in the SAP2000®'s implementation of the Nonlinear Modal History Analysis, also known as Fast Nonlinear Analysis (FNA). When the DI method is used for the response history analysis of a BI building, a global viscous damping matrix is formed as part of the solution to the equations of motion, which makes the mitigation of damping leakage a challenging task. This study provides solutions to address this challenge. The results of the FNA approach are used as a baseline to evaluate the applicability of the proposed solutions.

In many FE platforms, when implementing the DI method, for developing the global damping matrix, proportional damping coefficients are applied to the '*global*' mass and stiffness matrices of the system (for example this is the case when proportional damping is introduced through the Load Case in SAP2000®). Adopting this approach for a BI building results in a classical damping matrix. Furthermore, this global damping matrix is usually developed based on the elastic stiffness of the system (including isolators) and remains constant during the responses as opposed to being updated based on the current nonlinear stiffness of the system (isolators) at each time step. The combination of these two latter issues results in significant damping leakage to the isolated mode and the spurious suppression of the first-mode responses (up to 50% for the studied cases). Results of this research show that a nonclassical damping model (ie, the assembly of the superstructure and isolation system damping sub-matrices) might also fail to accurately specify the intended damping values to the vibration modes. Using the Rayleigh damping approach to develop the superstructure damping sub-matrix can lead to the undesired addition of damping to the first (isolated) mode arising from the mass-proportional component of the superstructure damping. In the isolated mode, the superstructure tends to move as a rigid body with no significant inter-story deformations.[27] Therefore, as identified in a few previous studies, the superstructure damping at the isolated mode is insignificant suggesting that the mass-proportional component of the superstructure damping should be removed from the global damping matrix to reliably capture the first-mode responses. The remaining challenge is the proper modeling of the viscous damping for the higher (superstructure) modes.

The higher-mode responses in a BI building are controlled by the superstructure inter-story deformations. Therefore, to achieve the desirable mitigation of the higher-mode responses, inter-story dashpots can be incorporated into the mathematical model of the building. The stiffness-proportional damping (KD) specified to the superstructure '*alone*' (ie, a nonclassical variant of the KD) can simulate this behavior. In this approach, the coefficient multiplying the superstructure stiffness matrix should be determined based on the second modal period of the BI building. The results of the response history analyses illustrate that this approach can properly assign the intended damping to the higher modes without imparting undesirable damping to the first mode. Therefore, this method can provide reliable estimates of the first- and higher-mode responses of BI buildings. It is worthwhile noting that, if in this method the stiffness matrix multiplier is based on the first mode (of either superstructure or BI structure) as recommended in a few previous studies, unrealistically large damping ratios are assigned to the higher modes resulting in the unintended suppression of the higher-mode responses (in some cases, higher-mode effects are virtually damped out). The desired nonclassical KD can be introduced to the numerical model through explicit viscous damper elements attached between adjacent floors. In a class of program such as SAP2000®, an alternative method to remove viscous damping from the isolated mode and specify viscous damping exclusively to the superstructure modes is the use of material damping.

ACKNOWLEDGMENT

The study presented in this paper was partially supported by a Dissertation Year Fellowship provided by the University of New Hampshire to the first author. This support is greatly appreciated. The authors would also like to thank the anonymous reviewers for their helpful and constructive comments that greatly contributed to improving the final version of the paper.

ORCID

Hamidreza Anajafi https://orcid.org/0000-0003-0397-2721

REFERENCES

1. Sarlis A, Constantinou M. *Modeling triple friction pendulum isolators in program SAP2000. Supplement to MCEER Report 05–009, document distributed to the engineering community together with example files*. Buffalo: University at Buffalo; 2010.
2. Computers and Structures Inc. SAP2000®: integrated finite element analysis and design of structures, version 20.2.0, software. Berkeley, CA; 2018.
3. Computers and Structures Inc. ETABS®: integrated building design, version 17.0.1, software. Berkeley, CA; 2018.
4. ABAQUS Inc., ABAQUS®, version 2018, software. Palo Alto, CA; 2018.
5. ANSYS Inc. ANSYS®, version 19.2, software. Canonsburg, PA; 2018.
6. McKenna F, Fenves GL, Scott MH. Open system for earthquake engineering simulation. Berkeley, CA: University of California; 2000.

7. Chopra AK.*Dynamics of structures: Theory and applications to earthquake engineering* (*4th edn*). Upper Saddle River, NJ: Prentice Hall; 2012.
8. Chen J, Zhao C, Xu Q, Yuan C. Seismic analysis and evaluation of the base isolation system in AP1000 NI under SSE loading. *Nucl Eng Des*.2014;278:117-133.
9. Kilar V, Petrovčič S, Koren D, Šilih S. Seismic analysis of an asymmetric fixed base and base-isolated high-rack steel structure.*Eng Struct*.2011;33(12):3471-3482.
10. Kilar V, Koren D.Seismic behaviour of asymmetric base isolated structures with various distributions of isolators. *Eng Struct*. 2009;31(4):910-921.
11. Fallah N, Zamiri G. Multi-objective optimal design of sliding base isolation using genetic algorithm. *Sci Iran*. 2013;20(1):87-96.
12. Pourzeynali S, Zarif M. Multi-objective optimization of seismically isolated high-rise building structures using genetic algorithms. *J Sound Vib*. 2008;311(3-5):1141-1160.
13. Tsai HC, Kelly JM. Seismic response of heavily damped base isolation systems. *Earthq Eng Struct Dyn*. 1993;22(7):633-645.
14. Chen M, Pantoli E, Wang X, et al. BNCS Report #1: Full-scale structural and nonstructural building system performance during earthquakes and post-earthquakefire-specimen design, construction and test protocol. *Structural Systems Research Project Report Series*, La Jolla, CA: University of California San Diego; 2013.
15. Chimamphant S, Kasai K. Comparative response and performance of base-isolated and fixed-base structures. *Earthq Eng Struct Dyn*. 2016;45(1):5-27.
16. Becker TC, Yamamoto S, Hamaguchi H, Higashino M, Nakashima M. Application of isolation to high-rise buildings: A Japanese design case study through a US design code lens. *Earthq Spectra*. 2015;31(3):1451-1470.
17. Anajafi H, Medina RA. Comparison of the seismic performance of a partial mass isolation technique with conventional TMD and base-isolation systems under broad-band and narrow-band excitations. *Eng Struct*. 2018;158:110-123.
18. Léger P, Dussault S. Seismic-energy dissipation in MDOF structures. *J Struct Eng*. 1992;118(5):1251-1269.
19. Charney FA. Unintended consequences of modeling damping in structures. *J Struct Eng*. 2008;134(4):581-592.
20. Erduran E. Evaluation of Rayleigh damping and its influence on engineering demand parameter estimates. *Earthq Eng Struct Dyn*. 2012;41(14):1905-1919.
21. Bernal D. Viscous damping in inelastic structural response. *J Struct Eng*. 1994;120(4):1240-1254.
22. Medina RA, Krawinkler H. Seismic demands for nondeteriorating frame structures and their dependence on ground motions. PEER Report 2003/15, *Pacific Earthquake Engineering Research Center*, Berkeley, CA; 2004.
23. Hall JF. Problems encountered from the use (or misuse) of Rayleigh damping. *Earthq Eng Struct Dyn*. 2006;35(5):525-545.
24. Zareian F, Medina RA. A practical method for proper modeling of structural damping in inelastic plane structural systems. *Comput Struct*. 2010;88(1-2):45-53.
25. Chopra AK, McKenna F. Modeling viscous damping in nonlinear response history analysis of buildings for earthquake excitation. *Earthq Eng Struct Dyn*. 2016;45(2):193-211.
26. Jehel P, Léger P, Ibrahimbegovic A. Initial versus tangent stiffness-based Rayleigh damping in inelastic time history seismic analyses. *Earthq Eng Struct Dyn*. 2014;43(3):467-484.
27. Ryan KL, Polanco J. Problems with Rayleigh damping in base-isolated buildings. *J Struct Eng*. 2008;134(11):1780-1784.
28. Dao ND, Ryan KL. Computational simulation of a full-scale, fixed-base, and isolated-base steel moment frame building tested at E-Defense. *J Struct Eng*. 2013;140(8):A4014005.
29. Kumar M, Whittaker AS, Constantinou MC. Seismic isolation of nuclear power plants using elastomeric bearings. Report No. MCEER R-15-0008, *Multidisciplinary Center for Earthquake Engineering Research*, Buffalo, NY; 2015.
30. Pant DR, Wijeyewickrema AC, ElGawady MA. Appropriate viscous damping for nonlinear time-history analysis of base-isolated reinforced concrete buildings. *Earthq Eng Struct Dyn*. 2013;42(15):2321-2339.
31. Kitayama S, Constantinou MC. Collapse performance of seismically isolated buildings designed by the procedures of ASCE/SEI 7. *Eng Struct.* 2018;164:243-258.
32. Kelly JM, Tsai HC. Seismic response of light internal equipment in base-isolated structures. *Earthq Eng Struct Dyn*. 1985;13(6):711-732.
33. Tsai HC, Kelly JM. Non-classical damping in dynamic analysis of base-isolated structures with internal equipment. *Earthq Eng Struct Dyn*. 1988;16(1):29-43.
34. Alhan C, Gavin H. A parametric study of linear and non-linear passively damped seismic isolation systems for buildings. *Eng Struct.* 2004;26(4):485-497.
35. Huang YN, Whittaker AS, Constantinou MC, Malushte S. Seismic demands on secondary systems in base-isolated nuclear power plants. *Earthq Eng Struct Dyn*. 2007;36(12):1741-1761.
36. Isaković T, Zevnik J, Fischinger M. Floor response spectra in isolated structures subjected to earthquakes weaker than the design earthquake—Part I: Isolation with high-damping rubber bearings. *Struct Control Health Monit*. 2011;18(6):635-659.
37. MathWork Inc. MATLAB R2018a, version 9.4, software, Natick, MA; 2018.

38. Kelly JM. The role of damping in seismic isolation. *Earthq Eng Struct Dyn*. 1999;28(1):3-20.
39. Anajafi H. Improved seismic design of non-structural components (NSCs) and development of nnovative control approaches to enhance the seismic performance of buildings and NSCs. Ph.D. Dissertation, Department of Civil and Environmental Engineering, University of New Hampshire, Durham, NH. 2018. Available at: https://pqdtopen.proquest.com/pubnum/10935426.html.
40. Anajafi H, Medina RA. Damping modification factor for elastic floor response spectra. *Bull Earthq Eng*. 2019;1-30. https://doi.org/10.1007/s10518-019-00684-3
41. Hall JF. The role of damping in seismic isolation. *Earthq Eng Struct Dyn*. 1999;28(12):1717-1720.
42. Wilson EL. *Static and dynamic analysis of structures* (*4th edn*). Berkeley, CA: Computers and Structures, Inc; 2004.
43. Giammona AP, Ryan KL, Dao ND. Evaluation of assumptions used in engineering practice to model buildings isolated with triple pendulum isolators in SAP2000. *Earthq Spectra*.2015;31(2):637-660.
44. Hwang J, Sheng L. Equivalent elastic seismic analysis of base-isolated bridges with lead-rubber bearings. *Eng Struct*. 1994;16(3):201-209.
45. ASCE (American Society of Civil Engineers). Minimum design loads and associated criteria for buildings and other structures. ASCE/SEI 7–2016, Roston, VA; 2016.

How to cite this article: Anajafi H, Medina RA, Bell ES. Effects of the improper modeling of viscous damping on the first-mode and higher-mode dominated responses of base-isolated buildings. *Earthquake Engng Struct Dyn*. 2019;1–22. https://doi.org/10.1002/eqe.3223